

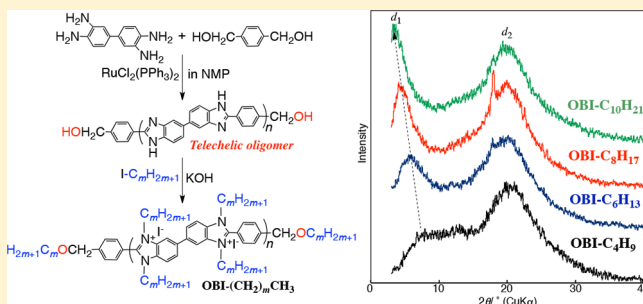
Ru-Complex-Catalyzed Synthesis of Telechelic Oligobenzimidazoles and Their Chemical Properties, Reactivity, and Structures

Isao Yamaguchi*¹ and Kohei Imoto

Department of Chemistry, Interdisciplinary Graduate School of Faculty of Science and Engineering, Shimane University, 1060 Nishikawatsu, Matsue 690-8504, Japan

Supporting Information

ABSTRACT: The reaction of 3,3'-diaminobenzidine (DAB) with 1,4-benzenedimethanol (BDM) in the presence of a $\text{RuCl}_2(\text{PPh}_3)_3$ catalyst yielded oligobenzimidazoles (OBIs) with OH groups at both ends. The degrees of oligomerization (DO) of the OBIs depended on the monomer feed ratio and reaction temperature. The reaction of the OBIs with $\text{CH}_3(\text{CH}_2)_m\text{I}$ ($m = 0, 3, 5, 7,$ and 9) assisted by KOH caused both N- and O-alkylation, yielding alkylated $\text{OBI}-(\text{CH}_2)_m\text{CH}_3$. The UV–vis measurements suggest that $\text{OBI}-\text{CH}_3$ forms a 1:2 charge transfer complex with 7,7,8,8-tetracyanoquinodimethane (TCNQ). The intensity of $\text{OBI}-\text{CH}_3$ photoluminescence decreased depending on the amount of TCNQ added to the solution. The quenching behavior was investigated by Stern–Volmer analysis. The OBIs and OBI-Rs were electrochemically oxidized and reduced. The powder X-ray diffraction patterns suggest that the OBI-Rs self-assemble into ordered structures in the solid state.



INTRODUCTION

Poly(benzimidazole)s (PBIs) and oligo(benzimidazole)s (OBIs) have attractive properties such as high thermal stability,^{1–3} proton conductivity,^{4–7} and affinity with nucleobases.^{8,9} Owing to these properties, they are used as materials for separation and proton exchange membranes in fuel cells^{10–16} as well as DNA and RNA binders.¹⁷ The synthesis of PBIs and OBIs usually requires severe conditions or the use of highly reactive monomers. For example, PBIs have been synthesized by the melting polycondensation of 3,3'-diaminobenzidine (DAB) with esters of aromatic dicarboxylic acids^{18–21} or by polycondensation of DAB tetrahydrochloride with aliphatic dicarboxylic acids using polyphosphoric acid as the dehydrating agent.²² Ionic PBIs have been synthesized by the chemical oxidation of poly(enetetramine)s, obtained by the polymerization of reactive benzimidazolium salts, under mild reaction conditions.^{23–25} The synthesis of PBIs and OBIs without reactive monomers under mild reaction conditions is advantageous regarding cost and environment concerns. Ruthenium complexes catalyze the condensation reactions of *o*-phenylenediamine with primary alcohols and with alkynes to afford 2-substituted benzimidazoles (BIs) without an acidic dehydrating agent.²⁶ We have applied these reactions to the polycondensation of DAB with α,ω -alkanediol,^{27,28} 1,1'-ferrocenedimethanol,²⁹ and α,ω -diynes³⁰ to afford functional PBIs.

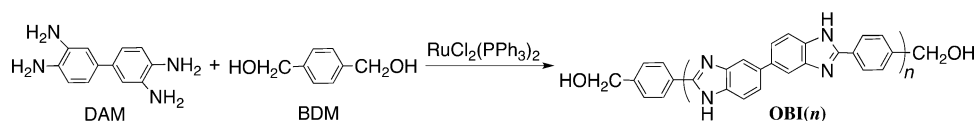
Conventional polycondensation reactions between two kinds of bifunctional monomers must be carried out in a 1:1 monomer feed ratio to achieve polymeric products in high yields. In contrast, the $\text{RuCl}_2(\text{PPh}_3)_3$ -catalyzed polycondensa-

tion of DAB with diols can occur in unbalanced feed ratios.^{27–29} The polycondensation of DAB with an excess of diols may afford telechelic products with OH end groups. In this study, the $\text{RuCl}_2(\text{PPh}_3)_3$ -catalyzed reaction of DAB with excess amounts of 1,4-benzenedimethanol (BDM) was carried out, and the structures, chemical properties, and reactivity of the obtained OBIs were investigated. Well-defined rigid rod oligomers have attracted considerable attention because they can be used to understand the chemical and physical properties of related polymeric materials as well as to investigate structure–property correlations.^{31–34} The OBIs with reactive NH, C=N, and OH groups can be modified by N- and O-alkylation reactions, and alkylated OBI-Rs will self-assemble into ordered structures in the solid state. It has been reported that rigid rod polymers and oligomers with long alkyl side chains often self-assemble into ordered structures in the solid state.^{35–47} The investigation of the structure–property correlations of such modified OBI-Rs can provide useful information for the development of new functional materials. To date, there have been no reports on telechelic OBIs, their applications as macromonomers, or OBI-Rs with self-assembled ordered structures. Herein, we report the Ru-complex-catalyzed synthesis of telechelic OBIs and their structures, chemical properties, and reactivity.

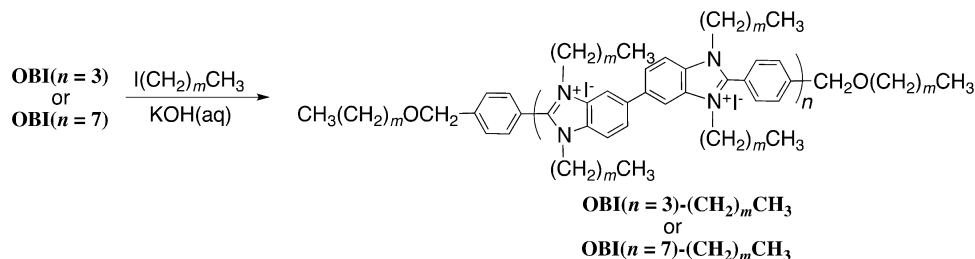
Received: October 11, 2017

Revised: December 8, 2017

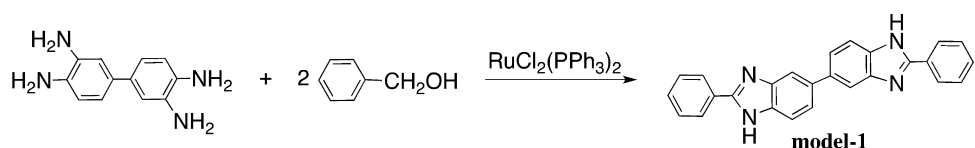
Scheme 1. Synthesis of OBIs



Scheme 2. Alkylation of OBI(n)S



Scheme 3. Synthesis of Model Compound



RESULTS AND DISCUSSION

Synthesis and Modification. The RuCl₂(PPh₃)₃-catalyzed reaction of DAB with BDM in 1:1, 1:1.5, 1:2, and 1:3 molar ratios at 190 °C yielded the oligobenzimidazoles OBI(*n* = 7), OBI(*n* = 5), OBI(*n* = 3), and OBI(*n* = 2), with DOs of 7.2, 5.4, 3.4, and 2.3, respectively (Scheme 1). In the reaction of *o*-phenylenediamine (PDA) with primary alcohols, the ruthenium complex acts as a dual catalyst for the oxidation of primary alcohols to aldehydes as well as for the cyclization of 2-iminoanilines, generated by the dehydration reaction of PDA with aldehydes, to the corresponding BIs.²³ It has been reported that the former catalytic reaction proceeds smoothly at a high reaction temperature.⁴⁸ Thus, the reaction of DAB with BDM in a 1:1 molar ratio was also carried out at 200 and 210 °C and resulted in yield of OBI(*n* = 12) and OBI(*n* = 22) with DOs of 11.5 and 21.5, respectively. The DO increase with increasing temperature in this oligomerization corresponds to a facile oxidation of BDM at high reaction temperatures. ESI TOF-MS analysis of OBI(*n* = 2) supports its terechelic structure (Figure S1).

Chemical modification of the OBIs was carried out by using reactive NH, C=N, and OH groups at both ends of the oligomers. The reaction of OBI(*n* = 3) and OBI(*n* = 7) with alkyl iodides (RI: CH₃(CH₂)_mI, *m* = 0, 3, 5, 7, and 9) assisted by KOH caused both N- and O-alkylation, yielding OBI(*n* = 3)-(CH₂)_mCH₃ and OBI(*n* = 7)-(CH₂)_mCH₃, respectively (Scheme 2). To compare the chemical properties of the oligomers, a model compound, model 1, was synthesized by the 1:2 reaction of DAB with benzyl alcohol (Scheme 3).

The OBIs obtained in this study are soluble in *N,N*-dimethylformamide (DMF) and dimethyl sulfoxide (DMSO). OBI(*n* = 3)-CH₃ and OBI(*n* = 7)-CH₃ are soluble in DMF and DMSO but insoluble in chloroform. On the other hand, OBI(*n* = 3)-(CH₂)_mCH₃ and OBI(*n* = 7)-(CH₂)_mCH₃ (*m* = 3, 5, 7, and 9) are insoluble in DMF and DMSO but soluble in chloroform because of the presence of hydrophobic long alkyl chains.

IR and ¹H NMR Spectra. Figure 1 shows the IR spectra of OBI(*n* = 3) and OBI(*n* = 3)-C₈H₁₇. Peaks corresponding to

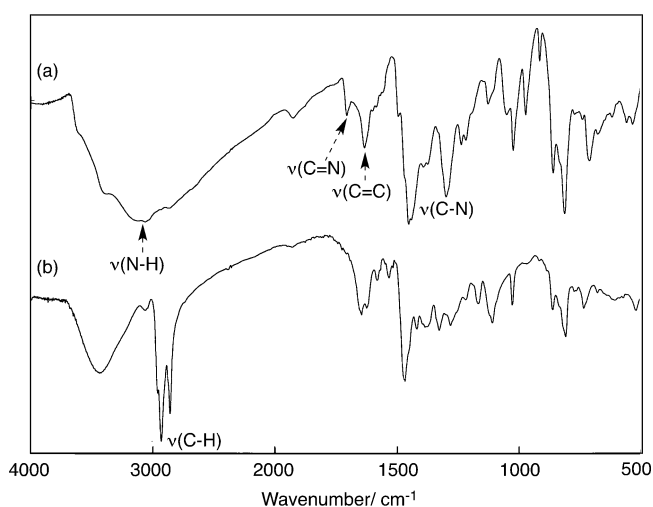


Figure 1. IR spectra of (a) OBI(*n* = 3) and (b) OBI(*n* = 3)-C₈H₁₇.

stretching vibrations of the C=N, C=C, and C–N bonds are observed at 1698, 1625, and 1290 cm⁻¹, respectively, in the IR spectrum of OBI(*n* = 3). A broad peak corresponding to stretching vibrations of the N–H bond is observed around 3400 cm⁻¹. The IR spectra of OBI(*n* = 7), OBI(*n* = 5), OBI(*n* = 4), and OBI(*n* = 2) are essentially the same as that of OBI(*n* = 3). Instead of the peaks corresponding to the stretching vibrations of the NH and C=N bonds, new peaks corresponding to the stretching vibrations of the hexyl group are observed in the range of 2853–2952 cm⁻¹ in the IR spectrum of OBI(*n* = 3)-C₈H₁₇.

Figure 2 shows the ¹H NMR spectra of OBI(*n* = 3), OBI(*n* = 22), and OBI(*n* = 3)-C₆H₁₃ in DMSO-*d*₆. The peak assignments are indicated in the figure. The peaks corresponding to the aromatic and methylene protons at both ends of

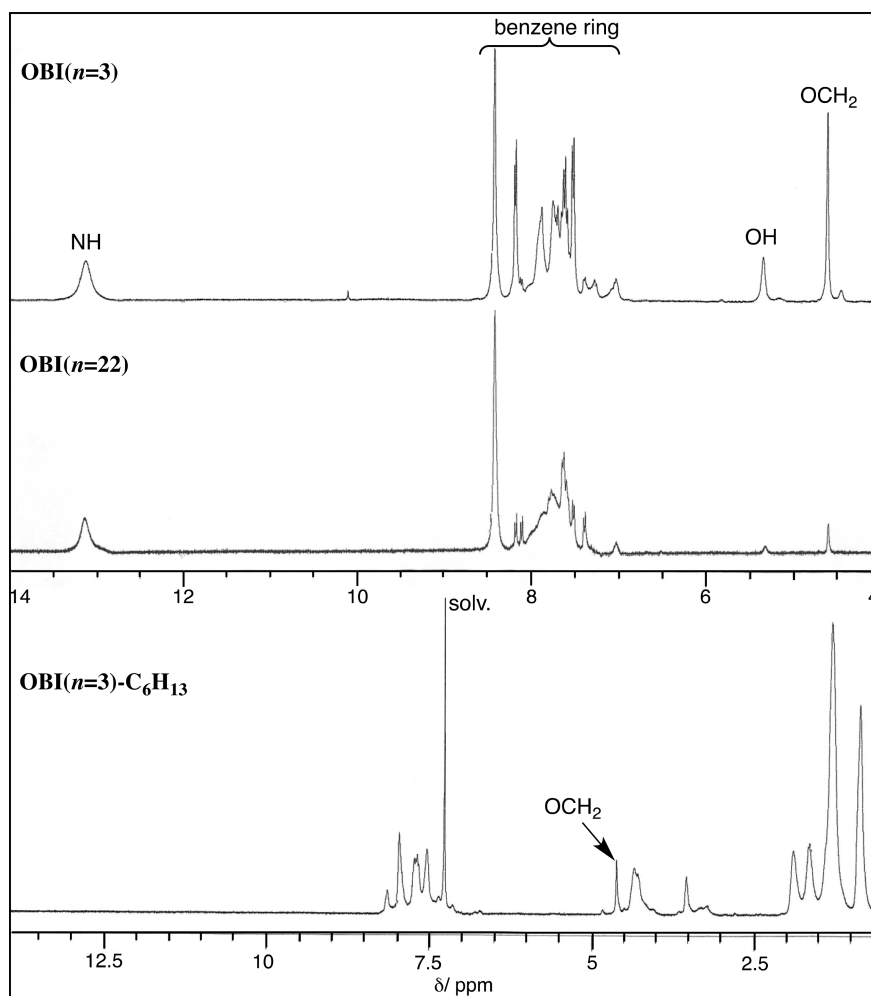


Figure 2. ^1H NMR spectra of $\text{OBI}(n = 3)$ and $\text{OBI}(n = 22)$ in $\text{DMSO}-d_6$ and $\text{OBI}(n = 3)-\text{C}_6\text{H}_{13}$ in CDCl_3 .

Table 1. Synthesis Results and Optical and Electrochemical Properties of Oligomers

	DAB:BDM	yield (%)	temp ($^{\circ}\text{C}$)	DO ^a	absorption (nm) ^b	photoluminescence (nm) ^c	E_{pa} (V ^d)	E_{pc} (V ^d)
$\text{OBI}(n = 7)$	1:1	76	190	7.2	266, 379	453 (0.14)	1.72	-1.58
$\text{OBI}(n = 5)$	1:1.5	83	200	5.4	265, 375	451 (0.47)	1.67	-1.46
$\text{OBI}(n = 3)$	1:2	96	190	3.4	265, 375	452 (0.44)	1.69	-1.41
$\text{OBI}(n = 2)$	1:3	72	190	2.3	265, 374	452 (0.49)	1.68	-1.32
$\text{OBI}(n = 12)$	1:1	85	200	11.5	266, 379	452 (0.16)	1.65	-1.46
$\text{OBI}(n = 22)$	1:1	85	210	21.5	266, 383	451 (0.23)	1.72	-1.36
model 1		30	190		268, 335	403 (0.62)		

^aDegree of oligomerization determined by the ^1H NMR spectrum. ^bIn DMSO . ^cIn DMSO . Quantum yield photoluminescence was shown in parentheses. ^dMeasured by cyclic voltammetry. Cast film on a Pt plate in an acetonitrile solution of $[\text{Et}_4\text{N}]\text{BF}_4$ (0.1 M). Sweep rate was 50 mV s^{-1} .

$\text{OBI}(n = 3)$ and $\text{OBI}(n = 22)$ are observed in the range approximately δ 7.0–8.4 and δ 4.6, respectively. The DO values were determined from the relative integral ratio of these peaks and are summarized in Table 1. The peaks corresponding to the NH and OH protons are observed at around δ 13.1 and δ 5.3, respectively, in the ^1H NMR spectra of $\text{OBI}(n = 3)$ and $\text{OBI}(n = 22)$. The assignment of the two peaks is confirmed by the fact that they disappeared on the addition of D_2O to the solutions. The two peaks corresponding to the NH and OH protons disappeared, and new peaks corresponding to the hexyl group appeared in the range δ 0.86–4.34 in the ^1H NMR spectrum of $\text{OBI}(n = 3)-\text{C}_6\text{H}_{13}$. The relative integral ratio of the peaks corresponding to the CH_2O groups at both ends and

the methyl protons of the hexyl groups suggests that the degree of both N- and O-hexylation of $\text{OBI}(n = 3)-\text{C}_6\text{H}_{13}$ is 0.95. The N- and O-alkylation of the other $\text{OBI}(n)$ -Rs also proceeded quantitatively, as summarized in Table 2.

Cyclic Voltammograms. Figure 3 shows cyclic voltammograms (CVs) of $\text{OBI}(n = 3)$ and $\text{OBI}(n = 3)-\text{C}_8\text{H}_{17}$ in an acetonitrile solution containing $[\text{Et}_4\text{N}]\text{BF}_4$ (0.10 M). $\text{OBI}(n = 3)$ exhibited a peak at 1.68 V (E_{pa} vs Ag^+/Ag) corresponding to electrochemical oxidation of the NH group. The peak disappeared in the CV of $\text{OBI}(n = 3)-\text{C}_8\text{H}_{17}$ because of the absence of the NH group in the octylated oligomer. As summarized in Table 1, the E_{pa} values are independent of the DOs of the oligomers. The results are consistent with the result

Table 2. Alkylation Degrees and Solid State Structural Data of OBI(*n*)-Rs

	yield (%)	alkylation degree (%) ^a	<i>d</i> ₁ (Å) ^b	<i>d</i> ₂ (Å) ^b
OBI(<i>n</i> = 3)-CH ₃	87	97		
OBI(<i>n</i> = 3)-C ₆ H ₉	36	97	10.8	4.4
OBI(<i>n</i> = 3)-C ₆ H ₁₃	40	95	15.0	4.4
OBI(<i>n</i> = 3)-C ₈ H ₁₇	24	87	18.6	4.3
OBI(<i>n</i> = 3)-C ₁₀ H ₂₁	38	100	25.7	4.3
OBI(<i>n</i> = 7)-CH ₃	26	85		
OBI(<i>n</i> = 7)-C ₆ H ₉	45	96	10.8	4.3
OBI(<i>n</i> = 7)-C ₆ H ₁₃	25	96	15.0	4.3
OBI(<i>n</i> = 7)-C ₈ H ₁₇	33	96	18.6	4.4
OBI(<i>n</i> = 7)-C ₁₀ H ₂₁	5	100	24.0	4.5

^aDetermined by the ¹H NMR spectrum. ^bDetermined by powder XRD measurements. *d*₁ = distance between the oligomer chains separated by alkyl chains. *d*₂ = face-to-face distance of the oligomer chain.

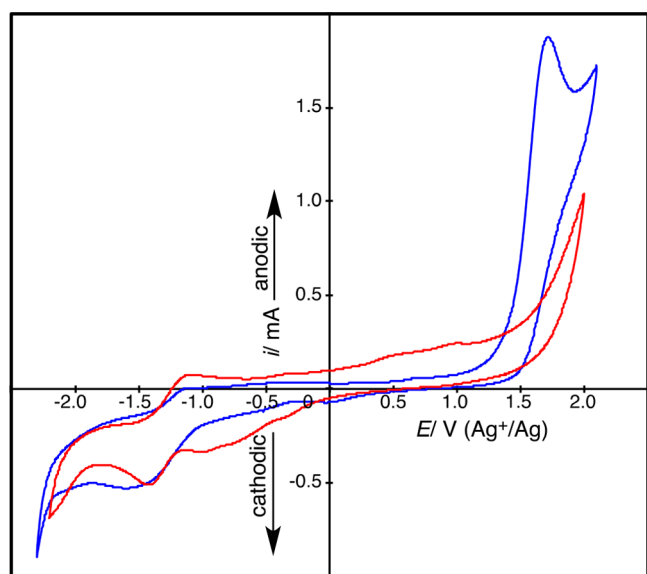


Figure 3. Cyclic voltammograms of cast film of OBI(*n* = 3) (blue curve) on a Pt plate and an acetonitrile solution containing OBI(*n* = 3)-C₈H₁₇ (red curve) and [Et₄N]BF₄ (0.10 M). Sweep rate was 50 mV s⁻¹.

that the λ_{\max} values of the oligomers are independent of their OPs. The fact that OBI(*n* = 3)-C₈H₁₇ exhibited an electrochemical reduction peak at a lower potential ($E_{\text{pc}} = -1.14$ V vs Ag⁺/Ag) than OBI(*n* = 3) ($E_{\text{pc}} = -1.41$ V vs Ag⁺/Ag) suggests that the imidazolium rings of OBI(*n* = 3)-C₈H₁₇ were more easily electrochemically reduced than the imidazole rings of OBI(*n* = 3). The lowest unoccupied molecular orbital (LUMO) energy levels of OBI(*n* = 3) and OBI(*n* = 3)-C₈H₁₇ were estimated to be -3.88 and -3.79 eV, respectively, according to the equation⁴⁹

$$\text{LUMO} = -(4.71 + E_{\text{pc}}^{\text{onset}})$$

where $E_{\text{pc}}^{\text{onset}}$ is the onset potential value of the reduction peak. The highest occupied molecular orbital (HOMO) energy levels of OBI(*n* = 3) and OBI(*n* = 3)-C₈H₁₇ were calculated by -6.76 and -6.52 eV, respectively, according to the equation

$$\text{HOMO} = -(E_{\text{g}}^{\text{opt}} - |\text{LUMO}|)$$

where $E_{\text{g}}^{\text{opt}}$ is the energy gap estimated from the onset wavelength of the absorption spectrum.

UV–Vis and Photoluminescence Spectra. Optical data are summarized in Table 1. Figure 4 shows the UV–vis spectra

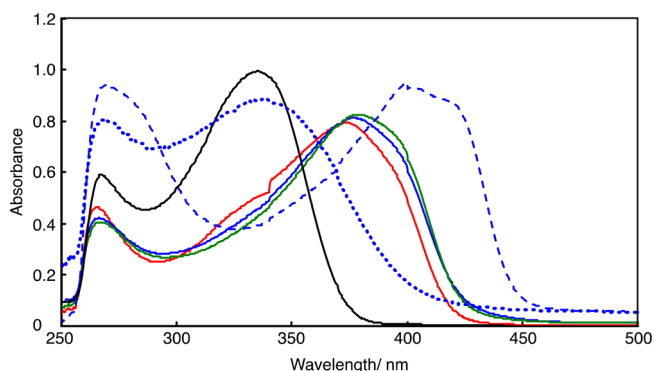


Figure 4. UV–vis spectra of OBI(*n* = 3) (red curve), OBI(*n* = 7) (blue solid curve), OBI(*n* = 12) (green curve), OBI(*n* = 7)-CH₃ (blue dotted curve), deprotonated OBI(*n* = 7) (blue hashed curve), and model 1 (black curve) in DMSO.

of OBI(*n* = 3), OBI(*n* = 7), OBI(*n* = 12), OBI(*n* = 7)-CH₃, deprotonated OBI(*n* = 3), and model 1 in DMSO. The oligomers show an absorption maximum (λ_{\max}) at a longer wavelength than that of model 1 because of the larger π -conjugation system in the oligomers. The fact that the λ_{\max} wavelengths of OBI(*n* = 3), OBI(*n* = 7), and OBI(*n* = 12) are essentially the same, irrespective of their DOs, indicates that the π -conjugation system is not expanded along the oligomer chain. This is probably due to a large degree of twisting between the benzimidazole and neighboring phenyl rings. It has been reported that the benzimidazole rings of 1,4-bis(2-benzimidazolyl)benzene are planar and lie at an angle of approximately 32° to the central phenyl ring.⁵⁰ The fact that the λ_{\max} of OBI(*n* = 7)-CH₃ is shorter than that of OBI(*n* = 7) corresponds to the assumption that the degree of twisting between the 1,3-dimethylbenzimidazolium and neighboring phenylene groups is larger than that between benzimidazole and neighboring phenylene groups.

The treatment of a DMSO solution of OBI(*n* = 3) with an excess amount of NaH caused a bathochromic shift of λ_{\max} by approximately 50 nm, as shown in Figure 4. This shift seems to be ascribed to the charge transfer from the N[−] anions generated via the deprotonation of the imidazole rings to the oligomer backbone. It has been reported that the deprotonation of OH group(s) of the aromatic compounds by NaH causes charge transfer from the O[−] anion to the inner aromatic rings, accompanied by a bathochromic shift of λ_{\max} .^{51–58}

The oligomers obtained in this study were photoluminescent in solution. The emission peak position of the oligomers ($\lambda_{\text{em}} = \text{ca. } 450$ nm) was longer than that of model 1 ($\lambda_{\text{em}} = 403$ nm) in solution. These observations are consistent with the facts that the λ_{\max} values of the oligomers are larger than that of model 1. The photoluminescence (PL) quantum yields (Φ) of the oligomers and model 1 are summarized in Table 1. The Φ value of model 1 was higher than those of the oligomers. The Φ values of the oligomers decreased as their DO values increased. Although reason for the results is unclear, they will be useful information for the development of new emissive materials.

Formation of CT Complex. It has been reported that TCNQ reacts with quaternary ammonium iodides to afford

charge transfer (CT) complexes.^{59–61} The reaction of OBI($n = 3$)-CH₃ or OBI($n = 7$)-CH₃ with TCNQ yielded CT complexes, namely OBI($n = 3$)-CH₃-TCNQ and OBI($n = 7$)-CH₃-TCNQ, respectively, while the reaction of OBI($n = 3$)-(CH₂) _{m} CH₃ ($m = 5$ and 7) with TCNQ resulted in the recovery of the substrates. The results correspond to the assumption that the long alkyl substituents of OBI($n = 3$)-(CH₂) _{m} CH₃ prevent the approach of TCNQ to the benzimidazolium ring.

Figure 5 shows the IR spectra of OBI($n = 3$)-CH₃-TCNQ and TCNQ. The fact that two peaks corresponding to

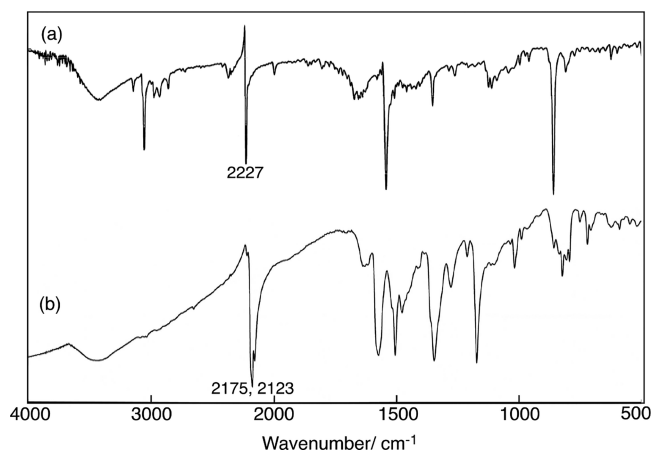


Figure 5. IR spectra of OBI($n = 3$)-CH₃-TCNQ and TCNQ.

stretching vibrations of the CN groups of OBI($n = 3$)-CH₃-TCNQ are observed at lower wavenumbers ($\nu_{\text{C}\equiv\text{N}} = 2123$ and 2175 cm^{-1}) than that of TCNQ ($\nu_{\text{C}\equiv\text{N}} = 2227 \text{ cm}^{-1}$) indicates that a CT complex was formed.

The addition of DMSO solutions of OBI($n = 3$)-CH₃ and OBI($n = 7$)-CH₃ to that of TCNQ caused spectral changes, particularly the appearance of new absorption peaks at approximately 350 nm and in the range 650–900 nm and the disappearance of the absorption peak at approximately 400 nm. Figure 6 shows the UV–vis spectral changes of OBI($n = 7$)-CH₃ in the presence of a series of concentrations of TCNQ. The absorptions in the range 650–900 nm corresponding to TCNQ radical anion, increased gradually with the addition of less than two equimolar quantities of TCNQ and remained almost unchanged after the addition of more than two

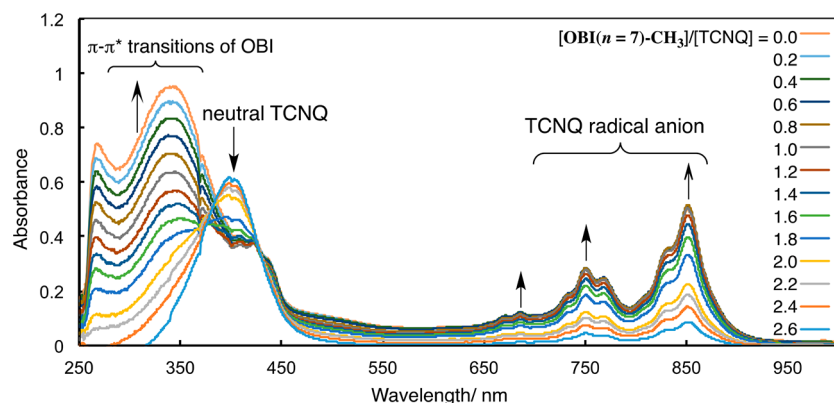


Figure 6. UV–vis spectral changes of the DMSO solution of TCNQ ($c = 1.5 \times 10^{-5} \text{ M}$) in the presence of a series of concentrations of OBI($n = 7$)-CH₃.

equimolar quantities of TCNQ. These observations suggest that OBI($n = 7$)-CH₃ forms a 1:2 CT complex with TCNQ. To confirm this assumption, the 1:2 modified Benesi–Hildebrand equation (eq 1)⁶² was employed to calculate the formation constant, K (L mol^{-1}), of the CT complex between TCNQ and OBI($n = 3$)-CH₃ or OBI($n = 7$)-CH₃:

$$(C_a)^2 C_d / A = 1 / K\epsilon + 1 / \epsilon C_a (4C_d + C_a) \quad (1)$$

where C_a and C_d are the initial concentrations of the acceptor and the donor, respectively, and A is the absorbance of the detected band ($\lambda = 755 \text{ nm}$). Figure 7 shows the 1:2 Benesi–

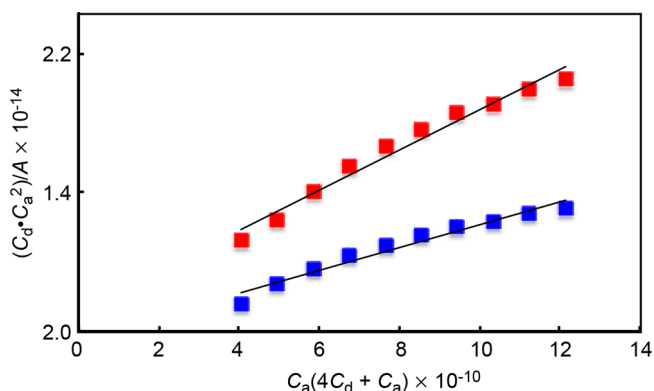


Figure 7. 1:2 Benesi–Hildebrand plots of OBI($n = 3$)-CH₃-TCNQ (red plots) and OBI($n = 7$)-CH₃-TCNQ (blue plots).

Hildebrand plots. By plotting the $(C_a)^2 C_d / A$ values as a function of the corresponding $C_a(4C_d + C_a)$ values, a straight line is obtained with a slope of $1/\epsilon$ and an intercept at $1/K\epsilon$, which indicates the formation of a 1:2 complex between OBI($n = 3$)-CH₃ or OBI($n = 7$)-CH₃ with TCNQ. The normalized K' values according to the average number of the benzimidazolium units (donor) in OBI($n = 3$)-CH₃-TCNQ and OBI($n = 7$)-CH₃-TCNQ were calculated to be 7.0×10^8 and $7.9 \times 10^8 \text{ L mol}^{-1}$, respectively. The larger K' value of OBI($n = 7$)-CH₃-TCNQ than OBI($n = 3$)-CH₃-TCNQ is probably due to the assumption that there is a larger content of the benzimidazolium unit (donor) in OBI($n = 7$)-CH₃-TCNQ than OBI($n = 3$)-CH₃-TCNQ, which makes it easier to form CT complexes with TCNQ (acceptor). In addition to Benesi–Hildebrand plots, Job's plot analysis was also carried out to confirm the 1:2 CT complexation between OBI($n = 7$)-CH₃ and TCNQ

(Figure 8). The Job plots display maxima at $[\text{OBI}(n = 7)\text{-CH}_3]/([\text{OBI}(n = 7)\text{-CH}_3] + [\text{TCNQ}]) = 0.67$, supporting 1:2 CT complex of $\text{OBI}(n = 7)\text{-CH}_3$ with TCNQ.

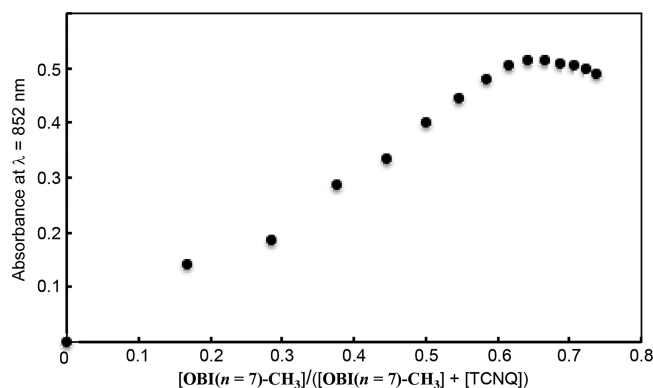


Figure 8. Job plots for $\text{OBI}(n = 3)\text{-CH}_3$ with TCNQ.

The PL peak intensities of $\text{OBI}(n = 3)\text{-CH}_3\text{-TCNQ}$ and $\text{OBI}(n = 7)\text{-CH}_3\text{-TCNQ}$ in DMSO decreased gradually depending on the amount of TCNQ added to the solutions. This result suggests that TCNQ acts as a PL quencher for the methylated oligomers. Recent studies of binary conjugated polymer blends highlight the competition between energy transfer and photoinduced charge transfer (PCT) events as a function of the HOMO and LUMO energy levels in the donor and acceptor pairs.^{63–65} When both the HOMO and LUMO energy levels are higher in one of the optical partners, donor excitation results in a PCT to the acceptor.^{66–71} As described above, the HOMO and LUMO energy levels of $\text{OBI}(n = 3)\text{-CH}_3\text{-TCNQ}$ are -6.70 and -3.88 eV, and those of $\text{OBI}(n = 7)\text{-CH}_3\text{-TCNQ}$ are -6.52 and -3.99 eV, respectively. These levels are higher than those of TCNQ (HOMO = -7.06 eV and LUMO = -4.48 eV).⁷² Figure 9 shows a possible PL quenching

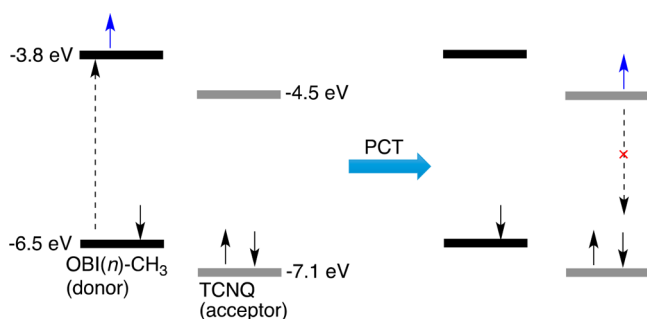


Figure 9. A possible quenching mechanism of methylated oligomer PL in the presence of TCNQ.

mechanism for the methylated oligomers in the presence of TCNQ. When the methylated OBI (donor) forms a CT complex with TCNQ (acceptor), donor excitation causes a PCT to the acceptor's LUMO. In this situation, the methylated oligomer PL is quenched. This assumption is confirmed by the fact that the PL intensity of $\text{OBI}(n = 3)$ is almost unchanged by the addition of TCNQ. Furthermore, the PL intensity of $\text{OBI}(n = 3)\text{-C}_6\text{H}_{13}$ is almost unchanged by the addition of TCNQ. The result corresponds to the fact that $\text{OBI}(n = 3)\text{-C}_6\text{H}_{13}$ does not form CT complex with TCNQ because the long hexyl pendant groups of $\text{OBI}(n = 3)\text{-C}_6\text{H}_{13}$, which are almost perpendicular to the oligomer backbone (cf. Powder X-ray

Diffraction section), prevent TCNQ from approaching to the imidazolium ring.

Figure 10 shows the PL spectra of $\text{OBI}(n = 7)\text{-CH}_3$ in the presence of a series of concentrations of TCNQ, which acts as a

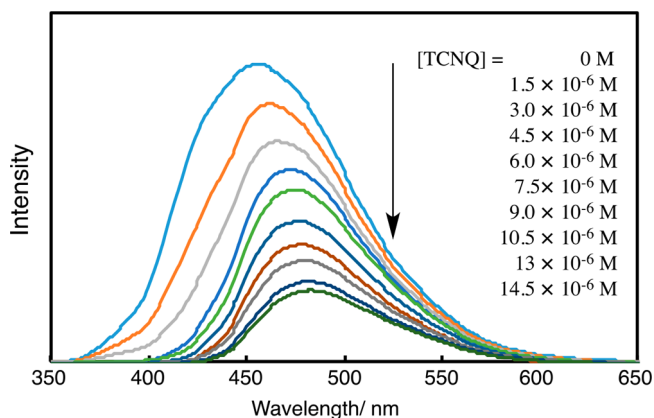


Figure 10. PL spectra of $\text{OBI}(n = 7)\text{-CH}_3$ in the presence of a series of concentrations of TCNQ.

PL quencher. The PL intensities decreased with increasing TCNQ concentration. A quantitative measurement of PL quenching can be achieved by determining the Stern–Volmer constant, K_{SV} , from the following equation: $I_0/I = 1 + K_{SV}[\text{quencher}]$, where I_0 is the PL intensity in the absence of quencher and I is the PL intensity in the presence of the quencher. This equation reveals that I_0/I increases in direct proportion to the concentration of the quenching moiety, and the constant K_{SV} defines the efficiency of quenching. Figure 11

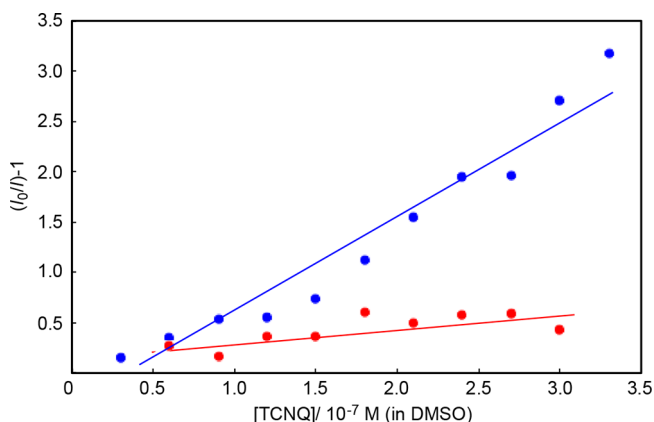


Figure 11. Stern–Volmer plots for PL quenching by TCNQ for $\text{OBI}(n = 3)\text{-CH}_3$ (red plots) and $\text{OBI}(n = 7)\text{-CH}_3$ (blue plots).

shows the Stern–Volmer plots for PL quenching by TCNQ for $\text{OBI}(n = 3)\text{-CH}_3$ and $\text{OBI}(n = 7)\text{-CH}_3$. The $K_{SV}(G)$ values of $\text{OBI}(n = 3)\text{-CH}_3$ and $\text{OBI}(n = 7)\text{-CH}_3$ are 1.4×10^6 and $9.8 \times 10^7 \text{ M}^{-1}$, respectively. The higher $K_{SV}(G)$ value of $\text{OBI}(n = 7)\text{-CH}_3$ compared to that of $\text{OBI}(n = 3)\text{-CH}_3$ can be attributed to the easier formation of a CT complex between $\text{OBI}(n = 7)\text{-CH}_3$ and TCNQ. The results are consistent with the results obtained from the 1:2 Benesi–Hildebrand plots in that the formation constant, K , between $\text{OBI}(n = 7)\text{-CH}_3$ and TCNQ is larger than that between $\text{OBI}(n = 3)\text{-CH}_3$ and TCNQ.

Powder X-ray Diffraction. Figure 12 shows powder X-ray diffraction (XRD) patterns of $\text{OBI}(n = 3)\text{-(CH}_2)_m\text{CH}_3$ ($m = 3$,

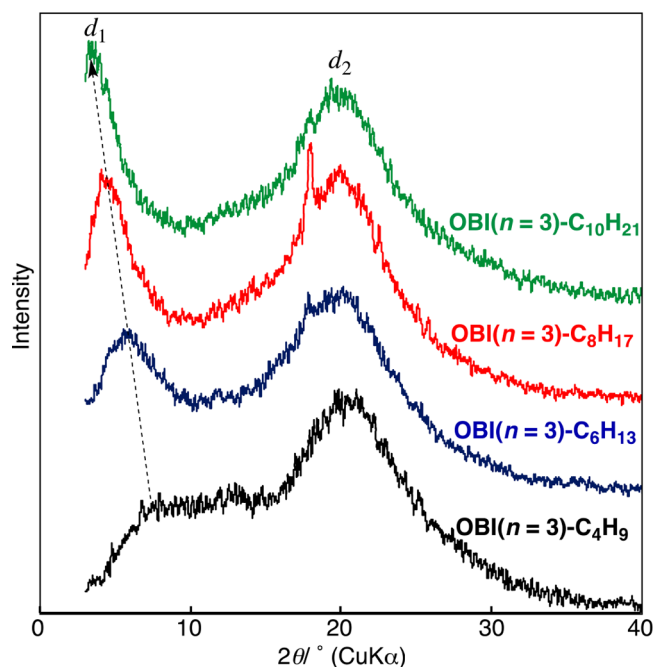


Figure 12. Powder XRD patterns of $\text{OBI}(n = 3)\text{-(CH}_2\text{)}_m\text{CH}_3$ ($m = 3, 5, 7,$ and 9).

$5, 7,$ and 9). The XRD patterns of the alkylated oligomers are similar to those of the π -conjugated oligomers and polymers with ordered structures in the solid state, exhibiting peak in the low-angle region and a medium intensity broad peak in the 2θ range of approximately $20^\circ\text{--}25^\circ$.³⁵ The former peak corresponds to the distances (d_1) between the oligomer chains separated by the alkyl side chains, while the latter corresponds to the face-to-face distance (d_2) of the oligomer chain.

The XRD patterns of $\text{OBI}(n = 3)\text{-C}_4\text{H}_9$, $\text{OBI}(n = 3)\text{-C}_6\text{H}_{13}$, $\text{OBI}(n = 3)\text{-C}_8\text{H}_{17}$, and $\text{OBI}(n = 3)\text{-C}_{10}\text{H}_{21}$ contain peaks at $2\theta = 8.2^\circ, 5.9^\circ, 4.7^\circ,$ and 3.4° corresponding to the distance ($d_1 = 10.8 \text{ \AA}$ for $\text{OBI}(n = 3)\text{-C}_4\text{H}_9$, $d_1 = 15.0 \text{ \AA}$ for $\text{OBI}(n = 3)\text{-C}_6\text{H}_{13}$, 18.6 \AA for $\text{OBI}(n = 3)\text{-C}_8\text{H}_{17}$, and 25.7 \AA for $\text{OBI}(n = 3)\text{-C}_{10}\text{H}_{21}$) between the oligomer chains separated by the alkyl side chains, and at $2\theta = 20.3^\circ, 20.1^\circ, 20.5^\circ,$ and 20.6° corresponding to the face-to-face distance of the oligomer chain ($d_2 = 4.3 \text{ \AA}$ for $\text{OBI}(n = 3)\text{-C}_4\text{H}_9$, $d_2 = 4.4 \text{ \AA}$ for $\text{OBI}(n = 3)\text{-C}_6\text{H}_{13}$, 4.3 \AA for $\text{OBI}(n = 3)\text{-C}_8\text{H}_{17}$, and 4.3 \AA for $\text{OBI}(n = 3)\text{-C}_{10}\text{H}_{21}$). The d_1 and d_2 values of $\text{OBI}(n = 7)\text{-(CH}_2\text{)}_m\text{CH}_3$ are essentially the same as those of $\text{OBI}(n = 3)\text{-(CH}_2\text{)}_m\text{CH}_3$. The d_1 and d_2 values of $\text{OBI}(n = 3)\text{-(CH}_2\text{)}_m\text{CH}_3$ and $\text{OBI}(n = 7)\text{-(CH}_2\text{)}_m\text{CH}_3$ ($m = 3, 5, 7,$ and 9) are summarized in Table 2. From previously reported $\text{CH}_2\text{--CH}_2$ distances (1.25 \AA) along the direction of the alkyl chain, the lengths of *n*-hexyl, *n*-hexyl, *n*-octyl, and *n*-decyl chains are estimated to be $5.0, 7.5, 10.0,$ and 12.5 \AA , respectively. The d_1 values of $\text{OBI}(n = 3)\text{-C}_4\text{H}_9$, $\text{OBI}(n = 3)\text{-C}_6\text{H}_{13}$, $\text{OBI}(n = 3)\text{-C}_8\text{H}_{17}$, and $\text{OBI}(n = 3)\text{-C}_{10}\text{H}_{21}$ are approximately double these values and increase proportionally with increasing alkyl chain length, as shown in Figure 13. The data suggest that the alkyl chains of the alkylated oligomers are almost perpendicular to the oligomer backbone with end-to-end packing structures in the solid state (Figure 14). The d_2 values of $\text{OBI}(n = 3)\text{-(CH}_2\text{)}_m\text{CH}_3$ and $\text{OBI}(n = 7)\text{-(CH}_2\text{)}_m\text{CH}_3$ ($m = 3, 5, 7,$ and 9) are comparable to those of self-assembled π -conjugated polymers, such as poly(hexyl-substituted *p*-phenyleneethynylene) ($d_2 = 3.8$ and 4.1 \AA),⁷³ with an end-to-end packing structure.

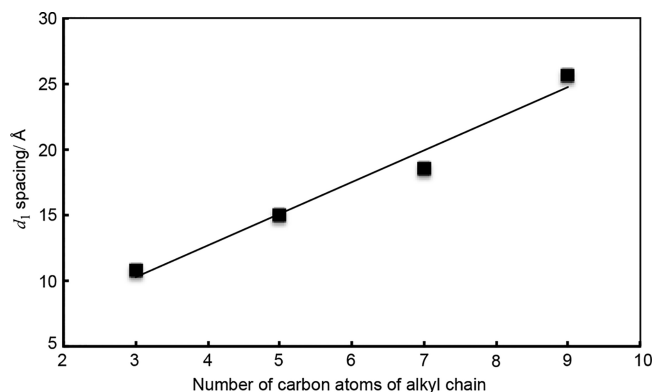


Figure 13. Plots of d_1 spacing between the main chains against the number of carbons (m) in the alkyl side chain for $\text{OBI}(n = 3)\text{-(CH}_2\text{)}_m\text{CH}_3$.

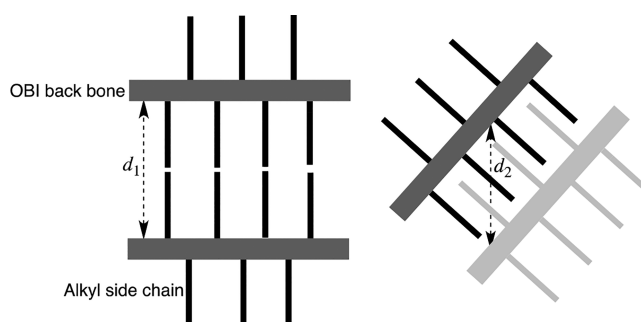


Figure 14. End-to-end packed structure.

CONCLUSIONS

The Ru-complex-catalyzed polycondensation of DAB with BDM yielded telechelic $\text{OBI}(n)$ s with OH groups at the both ends. The DOs of the OBIs depended on the monomer feed ratio and reaction temperature. The reaction of $\text{OBI}(n)$ s with alkyl iodides resulted in both N- and O-alkylation to yield alkylated $\text{OBI}(n)\text{-Rs}$. UV-vis analysis indicates that $\text{OBI}(n)\text{-CH}_3$ formed a 1:2 CT complex with TCNQ. The PL intensity of $\text{OBI}(n)\text{-CH}_3$ decreased on the addition of TCNQ, and the quenching effect of TCNQ is remarkable in the $\text{OBI}(n)\text{-CH}_3$ with larger n values. The powder X-ray diffraction patterns suggest that $\text{OBI}\text{-Rs}$ self-assembled into ordered structures in the solid state. From the results obtained in this study, we conclude that Ru-complex-catalyzed polycondensation will be useful for the development of reactive functional materials.

EXPERIMENTAL SECTION

General. Solvents were dried, distilled, and stored under nitrogen. Reagents were purchased and used without further purification. Reactions were carried out with standard Schlenk techniques under nitrogen.

IR and NMR spectra were recorded on a JASCO FT/IR-660 PLUS spectrophotometer with a KBr pellet and JEOL AL-400 and JEOL ECX-500 spectrometers, respectively. UV-vis and PL spectra were obtained by a JASCO V-560 spectrometer and a JASCO FP-6200, respectively. Cyclic voltammetry was performed with a Hokuto Denko HSV-110. $1 \text{ cm} \times 1$ and $1 \text{ cm} \times 2 \text{ cm}$ Pt plates and Pt wire were used as working, counter, and reference electrodes, respectively. Tetraethylammonium tetrafluoroborate was used as an electrolyte. Scan speed was 50 mV s^{-1} . Powder X-ray diffraction measurement was conducted using a Rigaku RINT 2500 generator with $\text{Cu K}\alpha$ irradiation.

Synthesis of $\text{OBI}(n = 3)$. $\text{RuCl}_2(\text{PPh}_3)_3$ (0.14 g, 0.15 mmol) was dissolved in *N*-methyl-2-pyrrolidone (NMP) (10 mL). To the solution

were added DAB (0.64 g, 3.0 mmol) and BDM (0.83 g, 6.0 mmol). After the reaction solution was stirred at 190 °C for 14 h, the solution was cooled to room temperature and stood for 4 h. The resulting precipitate was collected by filtration, dissolved in DMSO (2 mL), and reprecipitated from acetone (200 mL). The precipitate was collected by filtration and dried in vacuo to give OBI($n = 3$) as a light green powder (0.89 g, 96%). ^1H NMR (DMSO- d_6 , 400 MHz): δ 13.12 (4H), 7.03–8.43 (34H), 5.35 (2H), 4.60 (4H).

Other OBI(n)s were synthesized in a similar manner.

Data of OBI($n = 2$). ^1H NMR (DMSO- d_6 , 400 MHz): δ 13.2 (2H), 7.03–8.43 (24H), 5.36 (2H), 4.61 (4H).

Data of OBI($n = 5$). ^1H NMR (DMSO- d_6 , 400 MHz): δ 13.1 (5H), 7.02–8.43 (54H), 5.33 (2H), 4.60 (4H).

Data of OBI($n = 7$). ^1H NMR (DMSO- d_6 , 400 MHz): δ 13.1 (8H), 7.03–8.42 (74H), 5.33 (2H), 4.61 (4H).

Data of OBI($n = 11$). ^1H NMR (DMSO- d_6 , 400 MHz): δ 13.1 (13H), 7.03–8.42 (114H), 5.33 (2H), 4.61 (4H).

Data of OBI($n = 22$). ^1H NMR (DMSO- d_6 , 400 MHz): δ 13.1 (25H), 7.03–8.42 (224H), 5.32 (2H), 4.60 (4H).

Synthesis of OBI($n = 3$)-C₆H₁₃. After 1-iodobutane (2.49 g, 13.5 mmol) was added dropwise to the mixture of a DMSO (2 mL) solution of OBI($n = 3$) (0.22 g, 0.50 mmol) and an aqueous solution (2 mL) of KOH (5 M), the reaction solution was stirred at 45 °C for 16 h and extracted with chloroform. Chloroform of the organic layer was removed under vacuum, and the remaining DMSO solution was poured into hexane (300 mL). The precipitate was collected by filtration and dried under vacuum to give OBI($n = 3$)-C₆H₁₃ as a black solid (0.19 g, 40%). Degree of n -hexylation = 95%. ^1H NMR (CDCl₃, 400 MHz): δ 6.71–8.14 (36H), 4.61 (OCH₂, 4H), 4.34 (17.7H), 3.23–3.54 (8H), 1.29–1.89 (119H), 0.86 (CH₃, 44.5H).

Other alkylated OBI(n)-Rs were synthesized in a similar manner.

Data of OBI($n = 3$)-CH₃. Yield = 87%. Degree of methylation = 97%. ^1H NMR (CDCl₃, 400 MHz): δ 7.70–8.78 (34H), 4.59 (OCH₂, 4H), 3.96–4.71 (NCH₃, OCH₃, 45.4H).

Data of OBI($n = 3$)-C₄H₉. Yield = 36%. Degree of n -butylation = 98%. ^1H NMR (CDCl₃, 400 MHz): δ 6.71–8.14 (38H), 4.62 (OCH₂, 4H), 4.07–4.35 (18.4H), 3.26–3.55 (8.3H), 1.33–1.88 (61.2H), 0.92 (CH₃, 45.9H).

Data of OBI($n = 3$)-C₈H₁₇. Yield = 24%. Degree of n -octylation = 87%. ^1H NMR (400 MHz, CDCl₃): δ 6.71–8.14 (38H), 4.61 (OCH₂, 4H), 4.34 (16.7H), 3.22–3.54 (7H), 1.26–1.89 (166H), 0.87 (CH₃, 41H).

Data of OBI($n = 3$)-C₁₀H₂₁. Yield = 38%. Degree of n -decylation = 100%. ^1H NMR (CDCl₃, 400 MHz): δ 6.91–8.13 (38H), 4.61 (OCH₂, 4H), 4.33 (15.5H), 3.53 (12H), 1.24–1.89 (245H), 0.87 (CH₃, 46.6H).

Data of OBI($n = 7$)-CH₃. Yield = 57%. Degree of methylation = 97%. ^1H NMR (CDCl₃, 400 MHz): δ 7.70–8.33 (74H), 4.63 (OCH₂, 4H), 3.95–4.71 (CH₃, 89.7H).

Data of OBI($n = 7$)-C₄H₉. Yield = 45%. Degree of n -butylation = 96%. ^1H NMR (CDCl₃, 400 MHz): δ 6.72–8.14 (76H), 4.61 (OCH₂, 4H), 4.37 (24H), 3.30–3.75 (3.8H), 1.34–1.86 (115H), 0.91 (CH₃, 88.6H).

Data of OBI($n = 7$)-C₆H₁₃. Yield = 25%. Degree of n -hexylation = 96%. ^1H NMR (CDCl₃, 400 MHz): δ 6.70–8.13 (76H), 4.61 (OCH₂, 4H), 4.33 (25H), 3.21–3.63 (3.8H), 1.28–1.80 (233H), 0.86 (CH₃, 87.7H).

Data of OBI($n = 7$)-C₈H₁₇. Yield = 33%. Degree of n -octylation = 96%. ^1H NMR (CDCl₃, 400 MHz): δ 6.91–8.13 (76H), 4.61 (OCH₂, 4H), 4.33 (27H), 3.21–3.63 (3.8H), 1.26–1.89 (352H), 0.86 (CH₃, 88.5H).

Data of OBI($n = 7$)-C₁₀H₂₁. Yield = 5%. Degree of n -decylation = 100%. ^1H NMR (CDCl₃, 400 MHz): δ 6.83–8.14 (76H), 4.61 (OCH₂, 4H), 4.33 (24H), 3.21–3.65 (4H), 1.24–1.89 (489H), 0.86 (CH₃, 93.9H).

Synthesis of Model 1. RuCl₂(PPh₃)₃ (0.25 g, 0.26 mmol) was dissolved in NMP (10 mL). To the solution were added DAB (1.29 g, 6.0 mmol) and benzyl alcohol (3.9 g, 36 mmol). After the reaction solution was stirred at 200 °C for 14 h, the solvent was removed under vacuum. The resulting solid was washed with acetonitrile (300 mL),

collected by filtration, and dried in vacuo to give a light brown powder, which was dissolved in a mixture of chloroform and methanol. The precipitate from the solution was collected by filtration and dried in vacuo to give model 1 as a light brown powder (1.53 g, 66%). ^1H NMR (DMSO- d_6 , 400 MHz): δ 13.0 (br, 2H), 8.20–8.22 (m, 4H), 7.49–7.85 (m, 12H). ^{13}C NMR (DMSO- d_6 , 125 MHz): δ 151.78, 135.84, 130.09, 129.90, 128.97, 126.44, 122.00.

Synthesis of OBI($n = 3$)-CH₃-TCNQ. OBI($n = 3$)-CH₃ (0.10 g, 0.14 mmol) was dissolved in DMSO (2 mL). To the solution was added TCNQ (77 mg, 0.36 mmol). After the reaction solution was stirred at 20 °C for 7 h, the solvent was removed under vacuum. The resulting solid was washed with tetrahydrofuran (50 mL), collected by filtration, and dried in vacuo to give OBI($n = 3$)-CH₃-TCNQ as a black solid (0.12 g). IR (KBr, cm⁻¹): 2173 (s), 2155 (s), 1629 (w), 1571 (s), 1505 (s), 1475 (m), 1345 (s), 1277 (w), 1173 (s), 1016 (w), 822 (w).

OBI($n = 7$)-CH₃-TCNQ was synthesized in a similar manner. Data of OBI($n = 7$)-CH₃-TCNQ. ^1H NMR (DMSO- d_6 , 400 MHz): IR (KBr, cm⁻¹): 2178 (s), 2152 (s), 1637 (w), 1570 (s), 1504 (s), 1474 (m), 1345 (s), 1276 (m), 1173 (s), 1015 (w).

■ ASSOCIATED CONTENT

Supporting Information

The Supporting Information is available free of charge on the ACS Publications website at DOI: 10.1021/acs.macromol.7b02187.

ESI TOF-MS spectrum and TGA curves (PDF)

■ AUTHOR INFORMATION

Corresponding Author

*E-mail iyamaguchi@riko.shimane-u.ac.jp (I.Y.).

ORCID

Isao Yamaguchi: 0000-0003-2750-3110

Notes

The authors declare no competing financial interest.

■ ACKNOWLEDGMENTS

This work was performed under the Cooperative Research Program of “Network Joint Research Center for Materials and Devices” (No. 20171162).

■ REFERENCES

- (1) Li, D.; Shi, D.; Xia, Y.; Qiao, L.; Li, X.; Zhang, H. Superior Thermally Stable and Nonflammable Porous Polybenzimidazole Membrane with High Wettability for High-Power Lithium-Ion Batteries. *ACS Appl. Mater. Interfaces* **2017**, *9*, 8742–8750.
- (2) Mader, J.; Xiao, L.; Schmidt, T. J.; Benicewicz, B. C.; Brian, C. Polybenzimidazole/Acid Complexes as High-Temperature Membranes. *Adv. Polym. Sci.* **2008**, *216*, 63–124.
- (3) Sannigrahi, A.; Arunbabu, D.; Sankar, R. D.; Jana, T. Tuning the Molecular Properties of Polybenzimidazole by Copolymerization. *J. Phys. Chem. B* **2007**, *111*, 12124–12132.
- (4) Maity, M.; Jana, T. Polybenzimidazole Block Copolymers for Fuel Cell: Synthesis and Studies of Block Length Effects on Nanophase Separation, Mechanical Properties, and Proton Conductivity of PEM. *ACS Appl. Mater. Interfaces* **2014**, *6*, 6851–6864.
- (5) Hickner, M. A.; Ghassemi, H.; Kim, Y. S.; Einsla, B. R.; McGrath, J. E. Alternative Polymer Systems for Proton Exchange Membranes (PEMs). *Chem. Rev.* **2004**, *104*, 4587–4612.
- (6) Mecerreyes, D.; Grande, H.; Miguel, O.; Ochoteco, E.; Marcilla, R.; Cantero, I. Porous Polybenzimidazole Membranes Doped with Phosphoric Acid: Highly Proton-Conducting Solid Electrolytes. *Chem. Mater.* **2004**, *16*, 604–607.
- (7) Hoel, D.; Grunwald, E. High Protonic Conduction of Polybenzimidazole Films. *J. Phys. Chem.* **1977**, *81*, 2135–2136.

- (8) Meng, X. G.; Liu, L.; Zhou, C. S.; Wang, L.; Liu, C. L. Dinuclear Copper(II) Complexes of a Polybenzimidazole Ligand: Their Structures and Inductive Roles in DNA Condensation. *Inorg. Chem.* **2008**, *47*, 6572–6574.
- (9) Huang, X. Y.; Dong, X. W.; Li, X.; Meng, X. G.; Zhang, D.; Liu, C. L. Metal–polybenzimidazole complexes as a nonviral gene carrier: Effects of the DNA affinity on gene delivery. *J. Inorg. Biochem.* **2013**, *129*, 102–111.
- (10) Nicotera, I.; Kosma, V.; Simari, C.; Angioni, S.; Mustarelli, P.; Quartarone, E. Ion Dynamics and Mechanical Properties of Sulfonated Polybenzimidazole Membranes for High-Temperature Proton Exchange Membrane Fuel Cells. *J. Phys. Chem. C* **2015**, *119*, 9745–9753.
- (11) Subianto, S. Recent Advances in Polybenzimidazole/Phosphoric Acid Membranes for High-Temperature Fuel Cells. *Polym. Int.* **2014**, *63*, 1134–1144.
- (12) Zhang, H.; Shen, P. K. Recent Development of Polymer Electrolyte Membranes for Fuel Cells. *Chem. Rev.* **2012**, *112*, 2780–2832.
- (13) Lobato, J.; Cañizares, P.; Rodrigo, M. A.; Linares, J. J.; López-Vizcaino, R. Performance of a Vapor-Fed Polybenzimidazole (PBI)-Based Direct Methanol Fuel Cell. *Energy Fuels* **2008**, *22*, 3335–3345.
- (14) Li, Q.; Pan, C.; Jensen, J. O.; Noyé, P.; Bjerrum, N. J. Cross-Linked Polybenzimidazole Membranes for Fuel Cells. *Chem. Chem. Mater.* **2007**, *19*, 350–352.
- (15) Xiao, L.; Zhang, H.; Scanlon, E.; Ramanathan, L. S.; Choe, E.-W.; Rogers, D.; Apple, T.; Benicewicz, B. C. High-Temperature Polybenzimidazole Fuel Cell Membranes via a Sol–Gel Process. *Chem. Mater.* **2005**, *17*, 5328–5333.
- (16) Cheng, C. K.; Luo, J. L.; Chuang, K. T.; Sanger, A. R. Propane Fuel Cells Using Phosphoric-Acid-Doped Polybenzimidazole Membranes. *J. Phys. Chem. B* **2005**, *109*, 13036–13042.
- (17) Tanious, F. A.; Hamelberg, D.; Bailly, C.; Czarny, A.; Boykin, D. W.; Wilson, W. D. DNA Sequence Dependent Monomer-Dimer Binding Modulation of Asymmetric Benzimidazole Derivatives. *J. Am. Chem. Soc.* **2004**, *126*, 143–153.
- (18) Inoue, S.; Imai, Y.; Uno, K.; Iwakura, Y. Polybenzimidazoles and polybenzoxazoles containing alicyclic structures. *Makromol. Chem.* **1966**, *95*, 236–247.
- (19) Vogel, H.; Marvel, C. S. Polybenzimidazoles, New Thermally Stable Polymers. *J. Polym. Sci.* **1961**, *50*, 511–539.
- (20) Vogel, H.; Marvel, C. S. Polybenzimidazoles. II. *J. Polym. Sci., Part A: Gen. Pap.* **1963**, *1*, 1531–1541.
- (21) Plummer, L.; Marvel, C. S. Polybenzimidazoles. III. *J. Polym. Sci., Part A: Gen. Pap.* **1964**, *2*, 2559–2569.
- (22) Iwakura, Y.; Uno, K.; Imai, Y. Polybenzimidazoles. II. Polyalkylenebenzimidazoles. *Makromol. Chem.* **1964**, *77*, 33–40.
- (23) Kamplain, J. W.; Bielawski, C. W. Dynamic Covalent Polymers Based Upon Carbene Dimerization. *Chem. Chem. Commun.* **2006**, *42*, 1727–1729.
- (24) Tennyson, A. G.; Kamplain, J. W.; Bielawski, C. W. Oxidation of Poly(enetetramine)s: a New Strategy for the Synthesis of Conjugated Polyelectrolytes. *Chem. Chem. Commun.* **2009**, *45*, 2124–2126.
- (25) Coady, D. L.; Khramov, D. M.; Norris, B. C.; Tennyson, A. G.; Bielawski, C. W. Adapting N-Heterocyclic Carbene/Azide Coupling Chemistry for Polymer Synthesis: Enabling Access to Aromatic Polytriazenes. *Angew. Chem., Int. Ed.* **2009**, *48*, 5187–5190.
- (26) Kondo, T.; Yang, S.; Huh, K. T.; Kobayashi, M.; Kotachi, S.; Watanabe, Y. Ruthenium Complex-Catalyzed Facile Synthesis of 2-Substituted Benzo-azoles. *Chem. Lett.* **1991**, *20*, 1275–1278.
- (27) Yamaguchi, I.; Osakada, K.; Yamamoto, T. Preparation of Poly(alkylenebenzimidazole) by Ruthenium Complex Catalyzed Polycondensation of 3,3'-Diaminobenzidine with α,ω -Diols. *J. Polym. Sci., Part A: Polym. Chem.* **1999**, *37*, 1383–1392.
- (28) Yamaguchi, I.; Osakada, K.; Yamamoto, T. Polyrotaxane Containing a Blocking Group in Every Structural Unit of the Polymer Chain. Direct Synthesis of Poly(alkylenebenzimidazole) Rotaxane from Ru Complex Catalyzed Reaction of 1,12-Dodecanediol and 3,3'-Diaminobenzidine in the Presence of α -Cyclodextrin. *J. Am. Chem. Soc.* **1996**, *118*, 1811–1812.
- (29) Yamaguchi, I.; Osakada, K.; Yamamoto, T.; Katada, M. 1:2 Polycondensation of 3,3'-Diaminobenzidine and 1,1'-Ferrocenedimethanol Catalyzed by $\text{RuCl}_2(\text{PPh}_3)_3$ to Give Polybenzimidazole Containing Ferrocenylene Groups. *Bull. Chem. Soc. Jpn.* **1999**, *72*, 2557–2562.
- (30) Yamaguchi, I.; Osakada, K.; Yamamoto, T. Ru(0) Complex Catalyzed Polyaddition. New Synthesis of Poly(alkylenebenzoxazole) and Poly(alkylenebenzimidazole). *Polym. Bull.* **1999**, *42*, 141–147.
- (31) Schenning, A. P. H. J.; Meijer, E. W. Supramolecular Electronics; Nanowires from Self-assembled π -Conjugated Systems. *Chem. Commun.* **2005**, *42*, 3245–3258.
- (32) Carroll, R. L.; Gorman, C. B. The Genesis of Molecular Electronics. *Angew. Chem., Int. Ed.* **2002**, *41*, 4378–4400.
- (33) Martin, R. E.; Diederich, F. Linear Monodisperse π -Conjugated Oligomers: Model Compounds for Polymers and More. *Angew. Chem., Int. Ed.* **1999**, *38*, 1350–1377.
- (34) Tour, J. M. Conjugated Macromolecules of Precise Length and Constitution. Organic Synthesis for the Construction of Nanoarchitectures. *Chem. Rev.* **1996**, *96*, 537–554.
- (35) Sengmany, S.; Ceballos, C.; Belhadj, R.; Cachet-Vivier, C.; Gall, E. L.; Brissault, B.; Penelle, J.; Léonel, E. A Direct Route to Polythiophenes Displaying Lateral Substituents: Easy One-step Synthesis and Polymerization of Thiophene Monomers Substituted by a Dimethylenecarboxylate ($\text{CH}_2\text{CH}_2\text{COOR}$) Appendage on the 3-Position. *J. Polym. Sci., Part A: Polym. Chem.* **2012**, *50*, 900–911.
- (36) Lee, K. H.; Morino, K.; Sudo, A.; Endo, T. Preparation and Properties of a Novel Polythiophene, Poly[(3-hexyliminomethyl)thiophene] with a High Regioregularity. *J. Polym. Sci., Part A: Polym. Chem.* **2011**, *49*, 1190–1194.
- (37) Yamamoto, T.; Sato, T.; Iijima, T.; Abe, M.; Fukumoto, H.; Koizumi, T.; Usui, M.; Nakamura, Y.; Yagi, T.; Tajima, H.; Okada, T.; Sasaki, S.; Kishida, H.; Nakamura, A.; Fukuda, T.; Emoto, A.; Ushijima, H.; Kurosaki, C.; Hirota, H. Highly Coplanar Polythiophenes with $-\text{C}\equiv\text{CR}$ Side Chains: Self-assembly, Linear and Nonlinear Optical Properties, and Piezochromism. *Bull. Chem. Soc. Jpn.* **2009**, *82*, 896–909.
- (38) Kishida, H.; Hirota, K.; Wakabayashi, T.; Okamoto, H.; Kokubo, H.; Yamamoto, T. Third-order Optical Nonlinearity in Regio-controlled Polythiophene Films. *Appl. Phys. Lett.* **2005**, *87*, 121902.
- (39) Yamamoto, T.; Arai, M.; Kokubo, H.; Sasaki, S. Copolymers of Thiophene and Thiazole. Regioregulation in Synthesis, Stacking Structure, and Optical Properties. *Macromolecules* **2003**, *36*, 7986–7993.
- (40) Yamamoto, T.; Komarudin, D.; Arai, M.; Lee, B. L.; Suganuma, H.; Asakawa, N.; Inoue, Y.; Kubota, K.; Sasaki, S.; Fukuda, T.; Matsuda, H. Extensive Studies on π -Stacking of Poly(3-alkylthiophene-2,5-diyl)s and Poly(4-alkylthiazole-2,5-diyl)s by Optical Spectroscopy, NMR Analysis, Light Scattering Analysis, and X-ray Crystallography. *J. Am. Chem. Soc.* **1998**, *120*, 2047–2058.
- (41) Craley, C. R.; Zhang, R.; Kowalewski, T.; McCullough, R. D.; Stefan, M. C. Regioregular Poly(3-hexylthiophene) in a Novel Conducting Amphiphilic Block Copolymer. *Macromol. Rapid Commun.* **2009**, *30*, 11–16.
- (42) Osaka, I.; McCullough, R. D. Advances in Molecular Design and Synthesis of Regioregular Polythiophenes. *Acc. Chem. Res.* **2008**, *41*, 1202–1214.
- (43) Jeffries-El, M.; Sauvè, G.; McCullough, R. D. Facile Synthesis of End-functionalized Regioregular Poly(3-alkylthiophene)s via Modified Grignard Metathesis Reaction. *Macromolecules* **2005**, *38*, 10346–10352.
- (44) Iovu, M. C.; Sheina, E. E.; Gil, R. R.; McCullough, R. D. Experimental Evidence for the Quasi-“living” Nature of the Grignard Metathesis Method for the Synthesis of Regioregular Poly(3-alkylthiophenes). *Macromolecules* **2005**, *38*, 8649–8656.
- (45) Langeveld-Voss, B. M. W.; Waterval, R. J. M.; Janssen, R. A. J.; Meijer, E. W. Principles of “Majority Rules” and “Sergeants and

Soldiers" Applied to the Aggregation of Optically Active Polythiophenes: Evidence for a Multichain Phenomenon. *Macromolecules* **1999**, *32*, 227–230.

(46) Adachi, T.; Brazard, J.; Ono, R. J.; Hanson, B.; Traub, M. C.; Wu, Z. Q.; Li, Z.; Bolinger, J. C.; Ganesan, V.; Bielawski, C. W.; Vanden Bout, D. A.; Barbara, P. F. Regioregularity and Single Polythiophene Chain Conformation. *J. Phys. Chem. Lett.* **2011**, *2*, 1400–1404.

(47) Merlo, J. A.; Frisbie, C. D. Field Effect Transport and Trapping in Regioregular Polythiophene Nanofibers. *J. Phys. Chem. B* **2004**, *108*, 19169–19179.

(48) Murahashi, S.; Naota, T.; Ito, K.; Maeda, Y.; Taki, H. Ruthenium-Catalyzed Oxidative Transformation of Alcohols and Aldehydes to Esters and Lactones. *J. Org. Chem.* **1987**, *52*, 4319–4327.

(49) Zhang, G.; Fu, Y.; Xie, Z.; Zhang, Q. Low Bandgap Polymers with Benzo [1,2-b:4,5-b'] Dithiophene and Bisthiophene-dioxopyrrolothiophene Units for Photovoltaic Applications. *Polymer* **2011**, *52*, 415–421.

(50) Dudd, L. M.; Venardou, E.; Garcia-Verdugo, E.; Licence, P.; Blake, A. J.; Wilson, C.; Poliakoff, M. Synthesis of Benzimidazoles in High-temperature Water. *Green Chem.* **2003**, *5*, 187–192.

(51) Yamaguchi, I.; Yamaji, R. Synthesis of Hydroxyoligophenylenes Containing Electron-donating, Electron-accepting Groups, or π -Deficient Aromatic Ring and Their Solvatochromic Behavior. *J. Phys. Org. Chem.* **2017**, *30*, e3671.

(52) Yamaguchi, I.; Sato, K.; Okuno, M. Synthesis and Solvatochromic Behavior of Branched Oligophenylenes with Hydroxyl Groups. *J. Phys. Org. Chem.* **2014**, *27*, 622–627.

(53) Yamaguchi, I.; Sato, K. Synthesis and Solvatochromic Behavior of Pyrene Derivatives with 4-Hydroxyphenyl and 4-Hydroxyphenylethynyl Groups. *Bull. Chem. Soc. Jpn.* **2013**, *86*, 1174–1182.

(54) Yamaguchi, I.; Tsuchie, K. Synthesis and Solvatochromic Behavior of Hexaphenylbenzenes and Indeno[1,2-*b*]fluorene Derivatives with Hydroxyl Groups. *Int. J. Org. Chem.* **2012**, *2*, 178–187.

(55) Yamaguchi, I.; Mitsuno, J. Interamolecular Charge Transfer Induced by Deprotonation of Hydroxyl Group in π -Conjugated Polymers with π -Deficient Aromatic Rings. *React. Funct. Polym.* **2011**, *71*, 140–147.

(56) Yamaguchi, I.; Seo, K.; Kawashima, Y. Synthesis of Dihydroxyoligophenylenes Containing π -Deficient or π -Excess Hetero-aromatic Rings and Their Solvatochromic Behavior. *Tetrahedron* **2010**, *66*, 6725–6732.

(57) Yamaguchi, I.; Goto, K.; Sato, M. Enzyme and Transition-metal-complex Catalyzed Synthesis of Polyphenols Having Pendant Oligo(*p*-phenylene) and Their Optical and Electrochemical Properties. *Macromolecules* **2009**, *42*, 7836–7845.

(58) Yamaguchi, I.; Goto, K.; Sato, M. Synthesis of Oligophenylenes Containing Hydroxy Group and Their Solvatochromic Behavior. *Tetrahedron* **2009**, *65*, 3645–3652.

(59) Coulon, C.; Delhaes, P.; Flandrois, S.; Amiel, J.; Bonjour, E.; Dupuis, P. Physical Properties of Ternary Organic Conductors of TCNQ and Iodine: Role of the Counterions in the Low Temperature Instabilities. *J. Phys. (Paris)* **1985**, *46*, 783–792.

(60) Coulon, C.; Flandrois, S.; Delhaes, P.; Hauw, C.; Dupuis, P. Effect of Interchain Coulomb Interactions on the Metal-insulator Transition in Quasi-one-dimensional Systems: An Experimental Study Based on Homogeneous Series of Tetracyanoquinodimethane (TCNQ) Salts. *Phys. Rev. B: Condens. Matter Mater. Phys.* **1981**, *23*, 2850–2859.

(61) Torrance, J. B. The Difference Between Metallic and Insulating Salts of Tetracyanoquinodimethane (TCNQ): How to Design an Organic Metal. *Acc. Chem. Res.* **1979**, *12*, 79–86.

(62) Abu-Eittah, R.; Al-Sugeir, F. Charge Transfer Interaction of Bithienyls and Some Thiophene Derivatives with Electron Acceptors. *Can. J. Chem.* **1976**, *54*, 3705–3712.

(63) Halls, J. J. M.; Cornil, J.; dos Santos, D. A.; Silbey, R.; Hwang, D. H.; Holmes, A. B.; Brédas, J. L.; Friend, R. H. Resonant Multiple Andreev Reflections in Mesoscopic Superconducting Junctions. *Phys. Rev. B: Condens. Matter Mater. Phys.* **1999**, *60*, 5721.

(64) Segura, J. L.; Gómez, R.; Martin, N.; Luo, C.; Swartz, A.; Guldi, D. M. Variation of the Energy Gap in Fullerene-based Dendrons: Competitive versus Sequential Energy and Electron Transfer Events. *Chem. Commun.* **2001**, *8*, 707–708.

(65) Guldi, D. M.; Swartz, A.; Luo, C.; Gómez, R.; Segura, J.; Martin, N. Rigid Dendritic Donor–acceptor Ensembles: Control over Energy and Electron Transduction. *J. Am. Chem. Soc.* **2002**, *124*, 10875–10886.

(66) Liu, B.; Gaylord, B. S.; Wang, S.; Bazan, G. C. Effect of Chromophore-charge Distance on the Energy Transfer Properties of Water-soluble Conjugated Oligomers. *J. Am. Chem. Soc.* **2003**, *125*, 6705–6714.

(67) Liu, B.; Bazan, G. C. Optimization of the Molecular Orbital Energies of Conjugated Polymers for Optical Amplification of Fluorescent Sensors. *J. Am. Chem. Soc.* **2006**, *128*, 1188–1196.

(68) Sariciftci, N. S.; Smilowitz, L.; Heeger, A. J.; Wudl, F. Photoinduced Electron Transfer from a Conducting Polymer to Buckminsterfullerene. *Science* **1992**, *258*, 1474–1476.

(69) Xu, Q. H.; Moses, D.; Heeger, A. J. Time-resolved Measurements of Photoinduced Electron Transfer from Polyfluorene to C60. *Phys. Rev. B: Condens. Matter Mater. Phys.* **2003**, *67*, 245417.

(70) Brédas, J. L.; Beljonne, D.; Coropceanu, V.; Cornil, J. Charge-transfer and Energy-transfer Processes in π -Conjugated Oligomers and Polymers: a Molecular Picture. *Chem. Rev.* **2004**, *104*, 4971–5004.

(71) Thomas, K. R. J.; Thompson, A. L.; Sivakumar, A. V.; Bardeen, A. J.; Thayumanavan, S. Energy and Electron Transfer in Bifunctional Non-conjugated Dendrimers. *J. Am. Chem. Soc.* **2005**, *127*, 373–383.

(72) Srivastava, K. K.; Srivastava, S.; Alam, M. T.; Rituraj. Theoretical study of the effects of solvents on the ground state of TCNQ. *Adv. Appl. Sci. Res.* **2014**, *5*, 288–295.

(73) Huang, W. Y.; Gao, W.; Kwei, T. K.; Okamoto, Y. Synthesis and Characterization of Poly(alkyl-substituted *p*-phenylene ethynylene)s. *Macromolecules* **2001**, *34*, 1570–1578.